

## RECALIBRATION OF THE VIRIAL FACTOR AND $M_{\text{BH}} - \sigma_*$ RELATION FOR LOCAL ACTIVE GALAXIES

DAESEONG PARK<sup>1</sup>, BRANDON C. KELLY<sup>2</sup>, JONG-HAK WOO<sup>1,†</sup>, AND TOMMASO TREU<sup>2</sup>

<sup>1</sup>Astronomy Program, Department of Physics and Astronomy, Seoul National University, Seoul, 151-742, Republic of Korea; pds2001@astro.snu.ac.kr, woo@astro.snu.ac.kr and

<sup>2</sup>Department of Physics, University of California, Santa Barbara, CA 93106, USA; bckelly@physics.ucsb.edu, tt@physics.ucsb.edu

Accepted for publication in *ApJS*

### ABSTRACT

Determining the virial factor of the broad-line region (BLR) gas is crucial for calibrating AGN black hole mass estimators, since the measured line-of-sight velocity needs to be converted into the intrinsic virial velocity. The average virial factor has been empirically calibrated based on the  $M_{\text{BH}} - \sigma_*$  relation of quiescent galaxies, but the claimed values differ by a factor of two in recent studies. We investigate the origin of the difference by measuring the  $M_{\text{BH}} - \sigma_*$  relation using an updated galaxy sample from the literature, and explore the dependence of the virial factor on various fitting methods. We find that the discrepancy is primarily caused by the sample selection, while the difference stemming from the various regression methods is marginal. However, we generally prefer the FITEXY and Bayesian estimators based on Monte Carlo simulations for the  $M_{\text{BH}} - \sigma_*$  relation. In addition, the choice of independent variable in the regression leads to  $\sim 0.2$  dex variation in the virial factor inferred from the calibration process. Based on the determined virial factor, we present the updated  $M_{\text{BH}} - \sigma_*$  relation of local active galaxies.

*Subject headings:* galaxies: quiescent – galaxies: active – scaling relation – virial factor – regression methods

### 1. INTRODUCTION

Supermassive black holes (SMBHs) are thought to be ubiquitous in the centers of virtually all massive galaxies (e.g., Kormendy & Richstone 1995; Richstone et al. 1998; Ferrarese & Ford 2005). The close connection of black hole growth to galaxy evolution is inferred from the discovery of tight correlations between the masses of SMBHs ( $M_{\text{BH}}$ ) and the global properties of host galaxies, such as the stellar velocity dispersion ( $\sigma_*$ ; Ferrarese & Merritt 2000; Gebhardt et al. 2000) bulge luminosity ( $L_{\text{bul}}$ ; Magorrian et al. 1998; Marconi & Hunt 2003), and bulge mass ( $M_{\text{bul}}$ ; Häring & Rix 2004). The origin of these connections has been investigated in theoretical studies of galaxy evolution either through the introduction of active galactic nucleus (AGN) feedback (e.g., Kauffmann & Haehnelt 2000; Di Matteo et al. 2005; Croton et al. 2006; Hopkins et al. 2006; Bower et al. 2006; Somerville et al. 2008; Booth & Schaye 2009) or as simply being the result of a hierarchical merging framework (e.g., Peng 2007; Hirschmann et al. 2010; Janke & Maccio 2011). The interplay between the black holes and galaxies is now one of the basic ingredients in our understanding of galaxy formation and evolution.

In order to better understand the origin and evolution of the SMBH-host galaxy connection, AGN demographics, and the growth of the SMBHs through cosmic time, an accurate and precise measurement of black hole mass is essential. Stellar/gas dynamical modeling is commonly used to measure the black hole masses in quiescent galaxies. However, this technique requires high spatial resolution to resolve the sphere-of-influence of the black hole, thereby limiting it to the local universe. In active galaxies, the black hole mass can be determined by utilizing AGN variability. The reverberation mapping technique (Blandford & McKee 1982; Peterson 1993) has been used to estimate the mean size of the broad line region (BLR,  $R_{\text{BLR}}$ ) by cross-correlating the continuum light curve with the broad emission line light curve. Combining  $R_{\text{BLR}}$  with the line-of-sight velocity width ( $\Delta V$ ) measured from the variable component of the broad

emission line provides a virial black hole mass estimate as  $M_{\text{BH}} \equiv f \Delta V^2 R_{\text{BLR}} / G$ , where  $G$  is the gravitational constant and  $f$  is the virial factor that converts the measured virial product into the actual black hole mass. This technique is also limited to around 50 AGNs to date since it requires extensive photometric and spectroscopic monitoring observations. This technique has established the empirical size-luminosity relation (Wandel et al. 1999; Kaspi et al. 2000; Bentz et al. 2006a, 2009a), which is the basis for the single-epoch (SE) method. In the SE method, one simply substitutes the time-consuming BLR size measurement with AGN luminosity using the size-luminosity relation. This therefore provides estimates of black hole masses for broad line AGNs from a single spectroscopic observation, thus expanding the sample size substantially at any redshift. However, both methods suffer from the large uncertainty stemming from the unknown virial factor (see Park et al. 2012), which depends on the geometry and kinematics of BLR of individual AGNs.

Instead, an empirically calibrated average virial factor has been applied to most AGN black hole mass estimates, except for only a few objects where dynamical mass measurements can be obtained (e.g., Davies et al. 2006; Onken et al. 2007; Hicks & Malkan 2008). The first calibration of the virial factor was performed by Onken et al. (2004). They derived  $\langle f \rangle = 5.5 \pm 1.8$  based on a sample of 14 AGNs, for which both reverberation masses and stellar velocity dispersions were available, by forcing the AGN host galaxies to obey the same  $M_{\text{BH}} - \sigma_*$  relationship as for quiescent galaxies. By enlarging the dynamical range of the AGN sample, Woo et al. (2010) determined the virial factor as  $\log \langle f \rangle = 0.72^{+0.09}_{-0.10}$  (i.e.,  $\langle f \rangle = 5.2 \pm 1.2$ ) based on an updated reverberation sample of 24 AGNs, which included 8 low-mass local Seyfert 1 galaxies from the Lick AGN Monitoring project (Bentz et al. 2009b). They provided the upper limit of uncertainty in the derived virial factor as 0.43 dex based on the intrinsic scatter in the relation. In contrast, Graham et al. (2011) reported  $\langle f \rangle = 2.8^{+0.7}_{-0.5}$ , based on their updated  $M_{\text{BH}} - \sigma_*$  relation of quiescent galaxies, and an updated AGN sample, which is a factor of 2 smaller than the aforementioned values. Graham et al. (2011) commented that the value of  $\langle f \rangle$  might be even further

<sup>†</sup> Author to whom correspondence should be addressed.

lowered due to the effect of radiation pressure (see Marconi et al. 2008). This correspondingly reduces the black hole mass estimates for most AGNs by that amount, influencing all of the studies incorporating single-epoch AGN black hole masses. Thus it is important to investigate the origin of this difference and check for possible biases in the calibration process.

Since the derived  $M_{\text{BH}} - \sigma_*$  relation of quiescent galaxies is used to calibrate the virial factor in AGN mass estimators, under the assumption that the same  $M_{\text{BH}} - \sigma_*$  relation holds for AGN host galaxies, it is important to investigate the differences in the  $M_{\text{BH}} - \sigma_*$  relations of quiescent galaxies reported in the literature, and to study their effect on the derived virial factors. Originally the slopes of the  $M_{\text{BH}} - \sigma_*$  relation reported by Ferrarese & Merritt (2000) and Gebhardt et al. (2000) were  $4.8 \pm 0.5$  and  $3.75 \pm 0.3$  based on 12 and 26 galaxy samples, respectively. After that, various slopes have been reported in the literature, ranging from 3.68 to 5.95. Although the slopes are roughly consistent with the theoretical expectations of  $M \propto \sigma^5$  (Silk & Rees 1998) and  $M \propto \sigma^4$  (Fabian 1999), their difference and change are noteworthy. The possible origin of the difference in slopes has been investigated in the literature. The related factors are: (1) the type of regression method adopted (Tremaine et al. 2002; Novak et al. 2006; see Kelly 2007 for general applications of regression), (2) the size of the assigned uncertainty on the velocity dispersion (Merritt & Ferrarese 2001; Tremaine et al. 2002), (3) the velocity dispersion measures used (Tremaine et al. 2002), (4) the adopted value of velocity dispersion for the Milky Way (Merritt & Ferrarese 2001; Tremaine et al. 2002), (5) the spatial resolution of the data for the resolved BH sphere-of-influence (Ferrarese & Ford 2005; see also Gültekin et al. 2009, 2011; Batchelder 2010) (6) the morphological type of the sample used (Hu 2008; Graham 2008; Gültekin et al. 2009; Greene et al. 2010; Graham et al. 2011).

To understand the origin of the differences in the derived  $M_{\text{BH}} - \sigma_*$  relationships, we investigate in this work 3 main issues: the difference in samples, the difference in regression methods, and the direction of the regression analysis. Recently, with new measurements and improved modeling the number of dynamical mass measurements is continuously growing both at the high-mass and low-mass end regimes. To date, a total of 67 black hole masses in quiescent galaxies has been measured via stellar/gas/maser kinematics (see the most recent compilation from McConnell et al. 2011 and references therein). Therefore, it is presently a good time to investigate what effect the difference in samples has on the derived  $M_{\text{BH}} - \sigma_*$  relation using the largest sample ever. In addition, various estimators have been used for the regression analysis in the black hole scaling relation studies: FITEXY (e.g., Tremaine et al. 2002, Novak et al. 2006, Kim et al. 2008, Li et al. 2011, Beifiori et al. 2012, Vika et al. 2012, McConnell et al. 2011), BCES (e.g., Ferrarese & Merritt 2000, Ferrarese & Ford 2005, Hu 2008, Bentz et al. 2009a, Bennert et al. 2010, Graham et al. 2011), Maximum likelihood (e.g., Gültekin et al. 2009, Greene et al. 2010, Schulze & Gebhardt 2011), Bayesian approach (`linmix_err`) (e.g., Sani et al. 2011, Xiao et al. 2011, Mancini & Feoli 2012). Thus, in order to investigate the difference in the derived scaling relationships caused by the sample selection, it is important to investigate differences between the estimators for the  $M_{\text{BH}} - \sigma_*$  relation analysis. Finally, adopting the choice of independent variable is another issue for determining the  $M_{\text{BH}} - \sigma_*$  relation. Motivated by the suggestion by Graham et al. (2011) to use the ‘inverse’ fit to calibrate the single-epoch AGN mass estimates, we present results based on both of the forward and

inverse regressions.

This paper is organized as follows. In the next section, we describe the most commonly used regression methods in astronomy with their explicit implementations. In Section 3, we re-measure the  $M_{\text{BH}} - \sigma_*$  relation using 3 different samples from the literature and investigate the difference due to the regression methods and samples. In Section 4 we present our main result for the calibrated virial factors and discuss the difference based on the regression methods and samples. The difference from the direction of regression is discussed in Section 5. Finally, we summarize and conclude in Section 6.

## 2. LINEAR REGRESSION TECHNIQUES

Linear regression methods<sup>2</sup> in astronomy were exhaustively discussed in the pioneering paper, Isobe et al. (1990). They provided formulae for 5 unweighted bivariate linear regression coefficients with their error estimates, and recommended the bisector line for the case of treating the variables symmetrically. The second paper in the series, Feigelson & Babu (1992), extended their work by accommodating bootstrap and jackknife resampling procedures for error estimation, weighted regression, and truncated/censored regressions. In addition, they suggested practical strategies for linear regression problems in astronomy.

The BCES estimator (Bivariate Correlated Errors and intrinsic Scatter) was proposed by Akritas & Bershady (1996) in order to incorporate, heteroscedastic measurement errors, intrinsic scatter, and correlation in the measurement errors. The method of minimizing a  $\chi^2$  statistic (FITEXY), which account for measurement error in both the dependent and independent variable, was modified by Tremaine et al. (2002) to incorporate intrinsic scatter. They added the unknown constant intrinsic variance term in quadrature to the error of the dependent variable and determined it so that the reduced  $\chi^2$  is equal to a value of unity. Based on the Monte Carlo simulations performed by Tremaine et al. (2002) and Novak et al. (2006), they concluded that the modified FITEXY is a better estimator than the BCES. In particular, Tremaine et al. (2002) concluded that the BCES tends to be biased when the sample size is small or the mean square of the x errors is comparable to the variance of x distribution, and that it becomes inefficient when there is a single measurement with much larger error than others.

Kelly (2007) developed a sophisticated Bayesian linear regression technique, termed `linmix_err`. It accounts for intrinsic scatter in the relationship, heteroscedastic measurement errors in both the independent and dependent variables, and correlation between the measurement errors. This method uses a Gaussian mixture model for the distribution of independent variables, which is shown to work well particularly when the measurement errors are large by avoiding the bias incorporated if the choice of x-distribution model is incorrect (also noted in Auger et al. 2010). The method assumes that the measurement errors and intrinsic scatter are Gaussian, and it accommodates multiple independent variables, nondetections, and selection effects.

Recently, Gültekin et al. (2009) applied a maximum likelihood method to determine the  $M - \sigma$  and  $M - L$  relations by naturally incorporating an intrinsic scatter and upper limits. They also extensively investigated the distributional forms for the measurement error and intrinsic scatter. However, they did not include a model for the distribution of the independent variable, but instead used Monte Carlo sampling to assess the impact of the measurement errors in the indepen-

<sup>2</sup> For recent reviews, please see Hogg et al. (2010) and Caimmi (2011a,b).

dent variable on the parameter estimates.

To sum up, the four methods for linear regression that have been used to characterize the black hole/host galaxy scaling relationships are: (1) BCES (Akritas & Bershady 1996), (2) FITEXY (Tremaine et al. 2002), (3) Maximum likelihood (Gültekin et al. 2009), (4) LINMIX\_ERR (Kelly 2007). In this section we explicitly show our implementation and usage of each method. We assume the model of  $y = \alpha + \beta x$  in the following analysis.

### 2.1. BCES estimator

The BCES( $Y|X$ ) estimator is implemented using the formula described in Akritas & Bershady (1996),

$$\beta = \frac{\text{cov}(x, y) - \langle \sigma_{xy} \rangle}{\text{var}(x) - \langle \sigma_x^2 \rangle}, \quad (1)$$

$$\alpha = \langle y \rangle - \beta \langle x \rangle, \quad (2)$$

where  $\text{cov}(x, y)$  is the covariance of  $x$  and  $y$ ,  $\sigma_x$  is the standard deviation of the measurement error (i.e., standard measurement error) in  $x$ ,  $\text{var}(x)$  is the variance of  $x$ , and  $\sigma_{xy}$  is the covariance between the measurement errors in  $x$  and  $y$ . The intrinsic variance (i.e., variance in the intrinsic scatter) is estimated following the expression given in Cheng & Riu (2006) and Kelly (2007),

$$\sigma_{\text{int}} = \sqrt{\text{var}(y) - \langle \sigma_y^2 \rangle - \beta [\text{cov}(x, y) - \langle \sigma_{xy} \rangle]}. \quad (3)$$

The uncertainties in the parameters can be estimated with the bootstrap or using analytical estimates given in Akritas & Bershady (1996). In this work we assume  $\sigma_{xy} = 0$  (i.e., uncorrelated measurement errors), as most values of  $x$  and  $y$  in the  $M_{\text{BH}} - \sigma_*$  samples were independently measured and the covariances between the measurement errors are not provided in the literature. Thus, simply assuming the zero covariance seems to be more reasonable for these very heterogeneously collected  $M_{\text{BH}} - \sigma_*$  samples. In addition, there is no result incorporating the correlated measurement errors (i.e.,  $\sigma_{xy}$ ) to  $M_{\text{BH}} - \sigma_*$  fitting in the literature at least to our knowledge. Thus, to compare consistently with the results from the literature we here set  $\sigma_{xy} = 0$ .

### 2.2. FITEXY estimator

The FITEXY (Press et al. 1992), modified by Tremaine et al. (2002), is implemented in our work in IDL using the `mpfit` (Markwardt 2009) Levenberg-Marquardt least-squares minimization routine. Note that our implementation is basically similar to that given in Williams et al. (2010)<sup>3</sup>. It performs the linear regression by minimizing

$$\chi^2 = \sum_{i=1}^N \frac{(y_i - \alpha - \beta x_i)^2}{\sigma_{y,i}^2 + \beta^2 \sigma_{x,i}^2 + \sigma_{\text{int}}^2}, \quad (4)$$

where  $\alpha$  and  $\beta$  are the regression coefficients,  $\sigma_x$  and  $\sigma_y$  are the standard deviation in the measurement errors, and  $\sigma_{\text{int}}^2$  is the intrinsic variance. The value of  $\sigma_{\text{int}}$  is iteratively adjusted as an effective additional  $y$  error by repeating the fit until one obtains  $\chi^2/(N-2) = 1$  (i.e., following the suggested iterative procedure given in Bedregal et al. 2006 and Bamford et al. 2006). If after the initial iteration the reduced  $\chi^2$  is less than one, then no further iterations occur and one sets  $\sigma_{\text{int}} = 0$ . We estimate uncertainties in the regression parameters with the bootstrap method.

<sup>3</sup> <http://purl.org/mike/mpfitexy>

### 2.3. Maximum Likelihood estimator

The method of maximum likelihood is implemented similarly as given in Gültekin et al. (2009) (see also Woo et al. 2010). Under the assumptions of uncorrelated Gaussian measurement errors in both coordinates and Gaussian intrinsic scatter along  $y$ , the Gaussian likelihood function is given by

$$\mathcal{L} = \prod_{i=1}^N \frac{1}{\sqrt{2\pi\sigma_i^2}} \exp \left[ -\frac{(y_i - \alpha - \beta x_i)^2}{2\sigma_i^2} \right], \quad (5)$$

where

$$\sigma_i^2 = \sigma_{y,i}^2 + \beta^2 \sigma_{x,i}^2 + \sigma_{\text{int}}^2. \quad (6)$$

Note that this likelihood function implicitly assumes that the independent variable is uniformly distributed (i.e., a uniform prior for the intrinsic distribution of  $x$ ). Then the log-likelihood function is

$$\begin{aligned} -2 \ln \mathcal{L} &= \sum_{i=1}^N \ln (2\pi\sigma_i^2) + \sum_{i=1}^N \frac{(y_i - \alpha - \beta x_i)^2}{\sigma_i^2} \\ &= \sum_{i=1}^N \ln (2\pi\sigma_i^2) + \chi^2. \end{aligned} \quad (7)$$

This likelihood approach is more complete than the  $\chi^2$  method given in Equation (4) in a sense that it includes the intrinsic variance term in both the normalization and exponent of the likelihood function, and determines it simultaneously with the other regression coefficients. To estimate the best-fit parameters of  $(\alpha, \beta, \sigma_{\text{int}})$  using the maximum likelihood estimate (MLE), we minimize  $-2 \ln \mathcal{L}$  using the downhill simplex method implemented as AMOEBA (Press et al. 1992) in IDL. Then we adopt uncertainties in parameters as the average difference where  $\ln \mathcal{L}$  decreases from its maximum value by 0.5. We also estimate the parameter errors using the bootstrap method.

### 2.4. Bayesian estimator (`linmix_err`)

The Bayesian linear regression routine, `linmix_err`, developed by Kelly (2007) is available from the NASA IDL astronomy user's library<sup>4</sup>. Here we briefly summarize the method. For details, please refer to Kelly (2007).

This method assumes Gaussian intrinsic scatter, Gaussian measurement errors, and a weighted sum of  $K$  Gaussian functions for the distribution of the independent variable. The choice of a Gaussian mixture model was motivated in that it can not only approximate well various intrinsic distributions of the independent variable, but it is also a mathematically convenient conjugate family. The full measured data likelihood function is expressed as a mixture of bivariate normal distributions

$$\mathcal{L} = \prod_{i=1}^N \sum_{k=1}^K \frac{\pi_k}{2\pi |V_{k,i}|^{1/2}} \exp \left[ -\frac{1}{2} (z_i - \zeta_k)^T V_{k,i}^{-1} (z_i - \zeta_k) \right], \quad (8)$$

where  $\sum_{k=1}^K \pi_k = 1$  and the measured data, means, and covari-

<sup>4</sup> <http://idlastro.gsfc.nasa.gov/>

ance matrices are, respectively,

$$z_i = \begin{pmatrix} y_i \\ x_i \end{pmatrix}, \quad (9)$$

$$\zeta_k = \begin{pmatrix} \alpha + \beta \mu_k \\ \mu_k \end{pmatrix}, \quad (10)$$

$$V_{k,i} = \begin{pmatrix} \beta^2 \tau_k^2 + \sigma_{\text{int}}^2 + \sigma_{y,i}^2 & \beta \tau_k^2 + \sigma_{xy,i} \\ \beta \tau_k^2 + \sigma_{xy,i} & \tau_k^2 + \sigma_{x,i}^2 \end{pmatrix}. \quad (11)$$

In order to calculate the posterior probability distribution of the model parameters for the given measured data, it adopts uniform prior distributions on the regression parameters  $(\alpha, \beta, \sigma_{\text{int}}^2)$ . It also adopt a Dirichlet, normal, and scaled inverse- $\chi^2$  prior on the mixture model parameters  $(\pi_k, \mu_k, \tau_k^2)$ , respectively. The data is ‘fit’ using a Markov Chain Monte Carlo (MCMC) sampler. For each regression parameter, we take the best-fit value and uncertainty as the posterior median and posterior standard deviation from the marginal posterior distributions using the 100,000 random draws returned by the MCMC sampler. Note that the likelihood function given in Equation (8) converges to that of the maximum likelihood method given in Equation (5) if the distribution for the independent variable is assumed to be uniform rather than a mixture of normals and the measurement errors are uncorrelated.

As an illustration, we also used the likelihood function in the case of a single Gaussian model ( $K = 1, \pi_k = 1$ ) for the distribution of independent variable with uncorrelated measurement errors ( $\sigma_{xy,i} = 0$ ). For comparison with the procedure assuming a uniform intrinsic distribution (MLE) given in Section 2.3, we compute the maximum likelihood estimate (i.e.,  $\text{MLE}_{\text{IG}}$ ) utilizing the likelihood function derived from assuming the distribution of independent variable is a Gaussian.

In the following sections, we determine the  $\alpha, \beta$ , and  $\sigma_{\text{int}}$  parameters with the corresponding error estimates for the  $M_{\text{BH}} - \sigma_*$  relation using each regression technique described above.

### 3. THE $M_{\text{BH}} - \sigma_*$ RELATIONS

The  $M_{\text{BH}} - \sigma_*$  relation is generally expressed as the log-linear form,

$$\log(M_{\text{BH}}/M_{\odot}) = \alpha + \beta \log(\sigma_*/200 \text{ km s}^{-1}). \quad (12)$$

Here  $y = \log(M_{\text{BH}}/M_{\odot})$  and  $x = \log(\sigma_*/200 \text{ km s}^{-1})$ . We assume that the measurement errors in the logarithms of mass and stellar velocity dispersion are symmetric by taking the symmetric interval in log space, i.e.,  $\epsilon_{\log M_{\text{BH}}} = (\log M_{\text{BH}}^{\text{upper}} - \log M_{\text{BH}}^{\text{lower}})/2$  and  $\epsilon_{\log \sigma_*} = (\log \sigma_*^{\text{upper}} - \log \sigma_*^{\text{lower}})/2$ . Following Graham et al., for their data we assume that the measurement errors on the logarithm of mass are symmetric by taking the average of upper and lower  $1\sigma$  uncertainties on the linear scale and propagating it onto the logarithmic scale, i.e.,  $\epsilon_{\log M_{\text{BH}}} = 0.5 (e_{M_{\text{BH}}}^{\text{upper}} + e_{M_{\text{BH}}}^{\text{lower}}) / (M_{\text{BH}} \ln 10)$ . The measurement errors in the logarithm of the dispersion are  $\epsilon_{\log \sigma_*} = 0.5 (e_{\sigma_*}^{\text{upper}} + e_{\sigma_*}^{\text{lower}}) / (\sigma_* \ln 10)$ . However, note that this choice of error bars does not significantly affect our results.

#### 3.1. Re-measuring the relation with four methods

In this section we consistently re-derive the  $M_{\text{BH}} - \sigma_*$  relation using three literature samples to check our implementation of the fitting methods. Figure 1 shows the re-estimated  $M_{\text{BH}} - \sigma_*$  relations of the data from Gültekin et al. 2009 (*top*), McConnell et al. 2011 (*middle*), and Graham et al. 2011

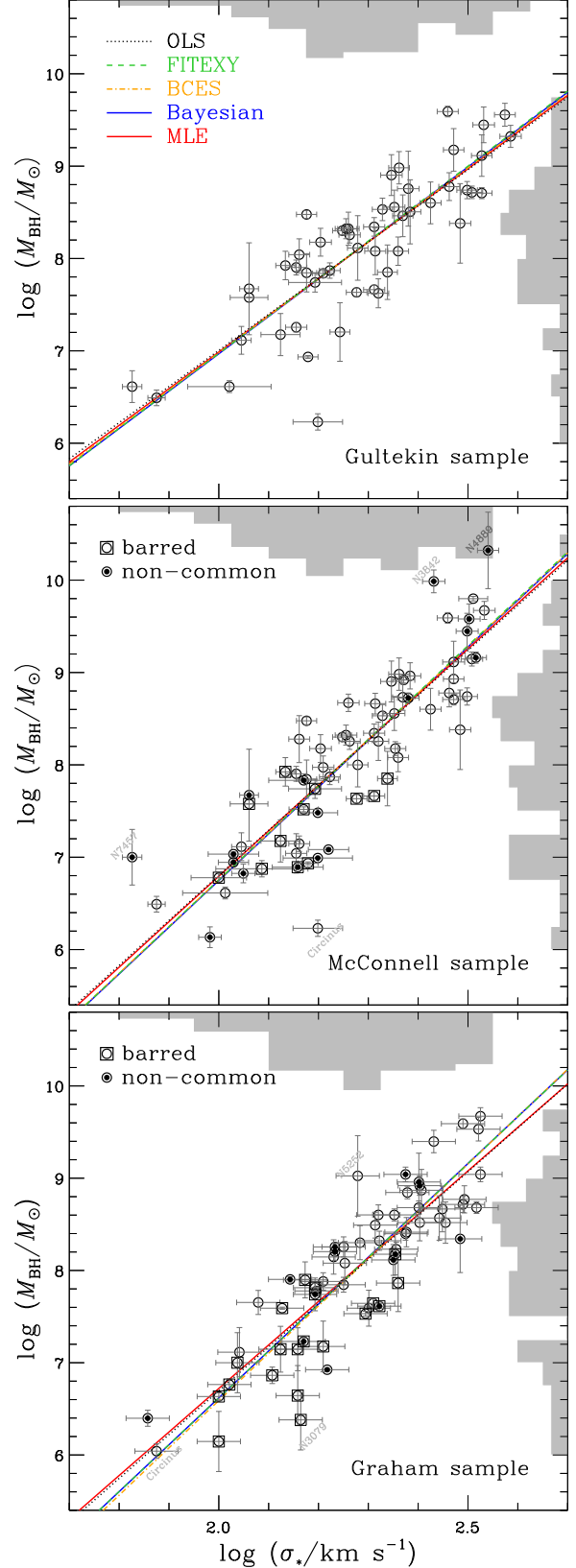


FIG. 1.— The  $M_{\text{BH}} - \sigma_*$  relations using each dataset from Gültekin et al. 2009 (*top*), McConnell et al. 2011 (*middle*), and Graham et al. 2011 (*bottom*). Each regression line is derived from five different methods (see the text and Table 1). The sample distributions for the logarithms of black hole masses and stellar velocity dispersions are shown in the right side and top side of each panel as grey histograms. The non-overlapping sample in between the McConnell and Graham data are marked with a filled dot inside open circles. Note that the common sample has 50 galaxies. The barred galaxies are marked with an open square enclosing open circles.

TABLE 1  
RE-ESTIMATION OF PARAMETERS FOR THE  $M_{\text{BH}} - \sigma_*$  RELATION OF QUIESCENT GALAXY SAMPLES:  
 $\log(M_{\text{BH}}/M_{\odot}) = \alpha + \beta \log(\sigma_*/200 \text{ km s}^{-1})$

Method	Forward regression			Inverse regression <sup>a</sup>		
	$\alpha$	$\beta$	$\sigma_{\text{int}}$	$\alpha = -\alpha_{\text{inv}}/\beta_{\text{inv}}$	$\beta = 1/\beta_{\text{inv}}$	$\sigma_{\text{int}} = \sigma_{\text{int,inv}}/\beta_{\text{inv}}$
Gültekin et al. (2009) Sample <sup>b</sup>						
OLS	$8.18 \pm 0.06$	$3.91 \pm 0.28$	...	$8.21 \pm 0.07$	$5.60 \pm 0.68$	...
MLE	$8.19 \pm 0.06$	$3.97 \pm 0.31$	$0.39 \pm 0.06$	$8.22 \pm 0.07$	$5.61 \pm 0.70$	$0.47 \pm 0.08$
BCES	$8.18 \pm 0.06$	$4.01 \pm 0.32$	$0.38 \pm 0.07$	$8.20 \pm 0.07$	$5.27 \pm 0.70$	$0.43 \pm 0.10$
FITEXY	$8.19 \pm 0.06$	$4.06 \pm 0.32$	$0.39 \pm 0.06$	$8.21 \pm 0.07$	$5.35 \pm 0.66$	$0.45 \pm 0.09$
Bayesian	$8.19 \pm 0.07$	$4.04 \pm 0.40$	$0.42 \pm 0.05$	$8.21 \pm 0.08$	$5.44 \pm 0.56$	$0.49 \pm 0.09$
McConnell et al. (2011) Sample <sup>c</sup>						
OLS	$8.27 \pm 0.06$	$4.87 \pm 0.37$	...	$8.33 \pm 0.06$	$6.55 \pm 0.50$	...
MLE	$8.28 \pm 0.06$	$4.92 \pm 0.34$	$0.41 \pm 0.05$	$8.33 \pm 0.06$	$6.43 \pm 0.51$	$0.47 \pm 0.06$
BCES	$8.28 \pm 0.06$	$5.06 \pm 0.41$	$0.43 \pm 0.05$	$8.33 \pm 0.06$	$6.36 \pm 0.51$	$0.48 \pm 0.07$
FITEXY	$8.28 \pm 0.06$	$5.07 \pm 0.36$	$0.43 \pm 0.05$	$8.32 \pm 0.06$	$6.29 \pm 0.49$	$0.47 \pm 0.06$
Bayesian	$8.27 \pm 0.06$	$5.06 \pm 0.36$	$0.44 \pm 0.05$	$8.32 \pm 0.07$	$6.31 \pm 0.46$	$0.49 \pm 0.07$
Graham et al. (2011) Sample						
OLS	$8.13 \pm 0.05$	$4.75 \pm 0.29$	...	$8.16 \pm 0.06$	$6.22 \pm 0.46$	...
MLE	$8.14 \pm 0.05$	$4.72 \pm 0.29$	$0.30 \pm 0.04$	$8.17 \pm 0.06$	$6.06 \pm 0.46$	$0.33 \pm 0.05$
BCES	$8.13 \pm 0.05$	$5.13 \pm 0.35$	$0.31 \pm 0.04$	$8.15 \pm 0.06$	$5.95 \pm 0.45$	$0.34 \pm 0.05$
FITEXY	$8.15 \pm 0.05$	$5.08 \pm 0.34$	$0.31 \pm 0.04$	$8.16 \pm 0.05$	$5.84 \pm 0.42$	$0.33 \pm 0.05$
Bayesian	$8.15 \pm 0.05$	$5.08 \pm 0.36$	$0.31 \pm 0.05$	$8.17 \pm 0.06$	$5.85 \pm 0.42$	$0.34 \pm 0.06$

NOTE. — Forward regression=fit  $\log M_{\text{BH}}$  on  $\log \sigma_*$ ; Inverse regression=fit  $\log \sigma_*$  on  $\log M_{\text{BH}}$ ; OLS=Ordinary Least Squares; MLE=Maximum Likelihood Estimates; BCES=estimator of Akritas & Bershady (1996); FITEXY=estimator of Tremaine et al. (2002); Bayesian=Bayesian posterior median estimates using `linmix_err` procedure of Kelly (2007).

<sup>a</sup> Inverse regression and its results will be discussed in Section 5.

<sup>b</sup> We used 49 galaxies listed in Table 1 in Gültekin et al. (2009) without upper limits for comparison with other samples. For the MLE estimate, we also estimate the parameters using the same likelihood function and error estimation method given in Gültekin et al. (2009). The result is  $(\alpha, \beta, \sigma_{\text{int}}) = (8.18 \pm 0.06, 3.97 \pm 0.39, 0.42 \pm 0.05)$ . Note that there are two different mass measurements for NGC 1399 and NGC 5128.

<sup>c</sup> We used all of the 67 galaxies listed in Table 4 in McConnell et al. (2011), while they used only 65. We found that there is a typo in the  $M_{\text{BH}}$  of NGC 1023 in their Table 4. Thus we corrected the value from  $14.6 \times 10^7$  to  $4.6 \times 10^7$ . Note that there are two different mass measurements for the NGC 1399 and for the NGC 5128. Following their scheme, if we apply half weights for them, then we get the same result with that of McConnell et al. (2011), i.e.,  $(\alpha, \beta, \sigma_{\text{int}}) = (8.28 \pm 0.06, 5.13 \pm 0.34, 0.42 \pm 0.05)$  for the FITEXY estimate.

(bottom) using the various methods described in the previous section. We also include the ordinary least squares (hereafter OLS) line as a reference. For the sample of 49 galaxies without upper limits from Table 1 in Gültekin et al. (2009), we also follow the same fitting scheme of their maximum likelihood estimator, which is slightly different to the method described in Section 2.3. Using the Gültekin et al. (2009) procedure, we first perform the fit without accounting for the measurement errors in the independent variables. Then, we incorporate the effects of measurement errors in  $x$  into the parameter uncertainties by adding in quadrature the standard deviations estimated from the Monte Carlo fitting results for  $10^4$  realizations of the independent variables. Recently, McConnell et al. (2011) have updated the compiled sample of 49 galaxies from Gültekin et al. (2009) by including new black hole mass measurements and revising earlier black hole masses based on improved stellar orbit modeling, which accounts for dark matter halos (Gebhardt & Thomas 2009; van den Bosch & de Zeeuw 2010; Shen & Gebhardt 2010; Schulze & Gebhardt 2011). We have consistently re-estimated slopes of the  $M_{\text{BH}} - \sigma_*$  relation using the 67 galaxies listed in Table 4 of McConnell et al. (2011). The independently compiled sample of 64 galaxies from Graham et al. (2011) is also used. Table 1 lists all regression results. Note that we get consistent results with each paper if we choose the same method and setting used by the respective papers.

For the Gültekin et al. sample the difference between fitted lines is only marginal since they assumed a minimum of 5% measurement errors on  $\sigma_*$ ; such small errors in  $\sigma_*$  are

found to have relatively small impact on the regression result, as described in the next section. However, the slope of the  $M_{\text{BH}} - \sigma_*$  relation derived from the updated sample of McConnell et al. is significantly larger than that of the Gültekin et al., increasing from  $\sim 4$  to  $\sim 5$ . As implied by the histograms for the black hole mass distributions shown in grey in the figures, this increase is mostly due to inclusion of both the low-mass and high-mass sample, which generally show an offset trend to the relation of the Gültekin et al. sample. For the Graham et al. sample the difference between fitted lines is marginally significant, and the slope is apparently divided into two groups, since they assigned relatively large (10%) measurement errors in  $\sigma_*$ . It seems that the bias of the maximum likelihood estimator starts to become non-negligible for  $x$ -errors of this magnitude. Therefore we investigate in details the effect of the amplitude of the  $x$ -error on these estimators in the following sections.

### 3.2. The effect of the adopted measurement uncertainty of $\sigma_*$

Merritt & Ferrarese (2001) first noted that ignoring the measurement errors in the velocity dispersion leads to a biased slope (i.e., underestimates) in the  $M_{\text{BH}} - \sigma_*$  relation. However, Tremaine et al. (2002) argued that the effect of the measurement errors in the velocity dispersion is not significant even at the 10% error level using two estimators, BCES and FITEXY, based on their simulation results. Indeed, the measurement errors in the independent variables can have significant impact on the regression analysis as also investigated by Kelly (2007), although the effect is only marginal in current

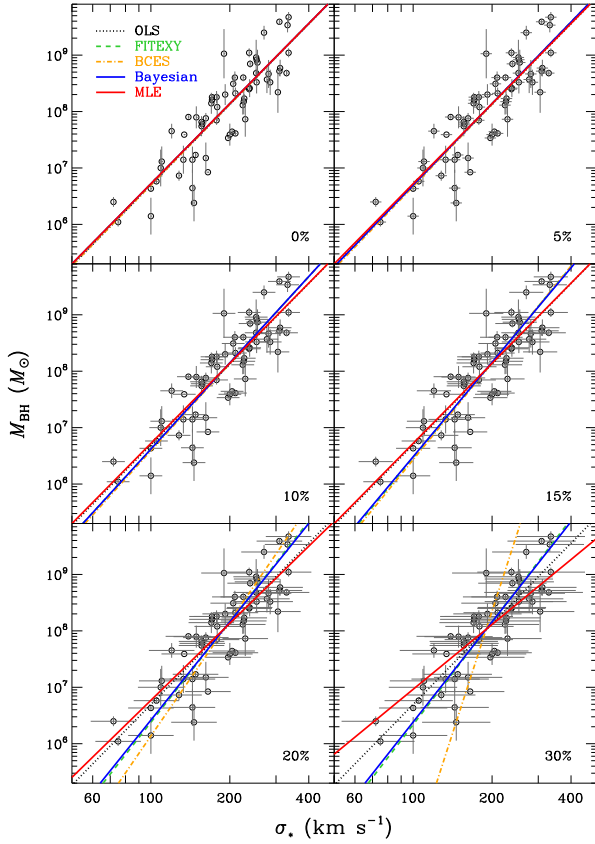


FIG. 2.— Comparison of five regression lines as a function of the assigned amount of measurement errors on  $\sigma_*$  using Graham et al. (2011) sample. The percentages of assigned errors are given at lower right corners in each panel. In the case of measurement errors on independent variables above 10%, the difference between the fitted lines is clearly visible.

datasets of the  $M_{\text{BH}} - \sigma_*$  relation. Typically the measurement errors in the velocity dispersion are assumed to be 5% or 10% in literature.

In Figure 2 we compare the fitted lines to the Graham et al.  $M_{\text{BH}} - \sigma_*$  dataset assuming measurement errors on  $\sigma_*$  ranging from 0% to 30%. The difference between the fitted lines is noticeable and obvious when the measurement errors are large. Figure 3 compares the regression coefficients and intrinsic scatter derived from the five estimators as a function of the assigned errors. As a reference we show the results from the OLS estimator, i.e., for the unweighted fitting scheme without accounting for the intrinsic scatter as described in Isobe et al. (1990). This estimator is biased when there are measurement errors.

For the intercept, the estimators do not give significantly different results except for the case of the BCES estimator. Both the intercept and slope estimated from the BCES estimator show very different behaviour in the high measurement error regime, which is consistent with the result from Tremaine et al. (2002).

For the slope, it is noted that all converge to the same value as the measurement errors in the velocity dispersion approach zero. Moreover, the estimators BCES, FITEXY, and Bayesian are very similar up to the 15% error level, thus indicating consistent estimation for these three estimators. The value of the slope from the BCES estimator becomes higher compared to the others as the assumed errors on  $\sigma_*$  increase. This is expected from the denominator term in Equation (1). As can be seen, the estimated slope from the maximum likelihood estimator is almost identical to the

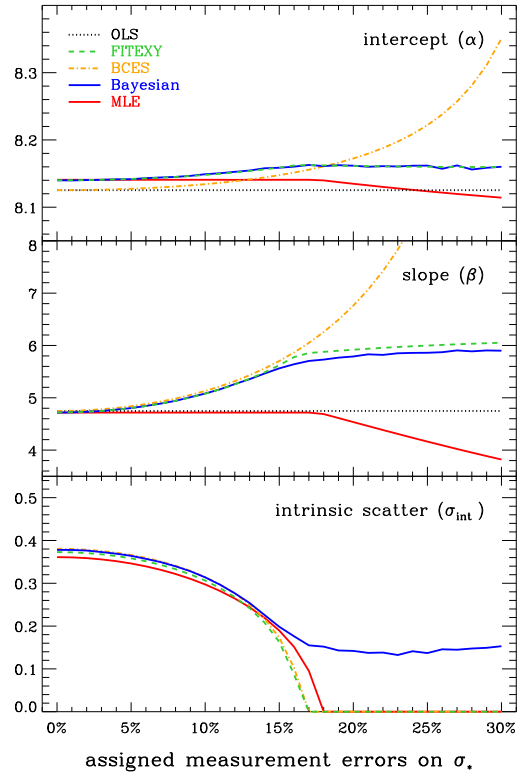


FIG. 3.— Direct comparison of regression results for the intercept (*top*), slope (*middle*), and intrinsic scatter (*bottom*) from the analysis of Figure 2. For the 5% errors the difference is only marginal. When the measurement errors are larger than 15% there is significant deviation between the estimators.

OLS result up to measurement error amplitudes of  $\sim 16\%$  on the independent variable. As noted and discussed in Kelly (2007) this biased behaviour is due to the implicit adoption of a naive uniform prior for the intrinsic distribution of the independent variables; this bias is also noted in K rding et al (2006). Based on this, we do not recommend the maximum likelihood method as outlined in Section 2.3. It is surprising that the FITEXY with an ad hoc iterative approach gives fairly consistent results with that of the fully Bayesian approach (`linmix_err`). This is inconsistent with the result of the simulations performed by Kelly (2007). The source of this discrepancy is that for the FITEXY estimator Kelly (2007) did not refit the slope and intercept each time after the intrinsic scatter term is iteratively adjusted (see also, Kelly 2011). Instead, he just assigned the intrinsic scatter value such that the reduced  $\chi^2$  is equal to unity using the first minimization result of  $\alpha$  and  $\beta$  for the zero intrinsic scatter case (i.e., just simply increasing  $\sigma_{\text{int}}$  without re-optimization each time).

For the intrinsic scatter, its level is very sensitive to the magnitude of the assumed measurement errors. Only `linmix_err` recovers a non-zero intrinsic scatter amplitude even in the case of assuming large measurement errors on  $\sigma_*$ .

### 3.3. Monte Carlo simulations

An incorrect model for the distribution of the true values of  $x$  and  $y$  can lead to biased slope estimates, especially in the case of relatively large measurement errors on the independent variables, as pointed out by Gull (1989) and Kelly (2007) (see also, Auger et al. 2010, Mantz et al. 2010, and March et al. 2011). Here we use Monte Carlo simulations to investigate the effect of an incorrect assumption on the intrinsic distribution of the independent variables. First, we generate three 10,000 simulated datasets by assuming respectively uni-

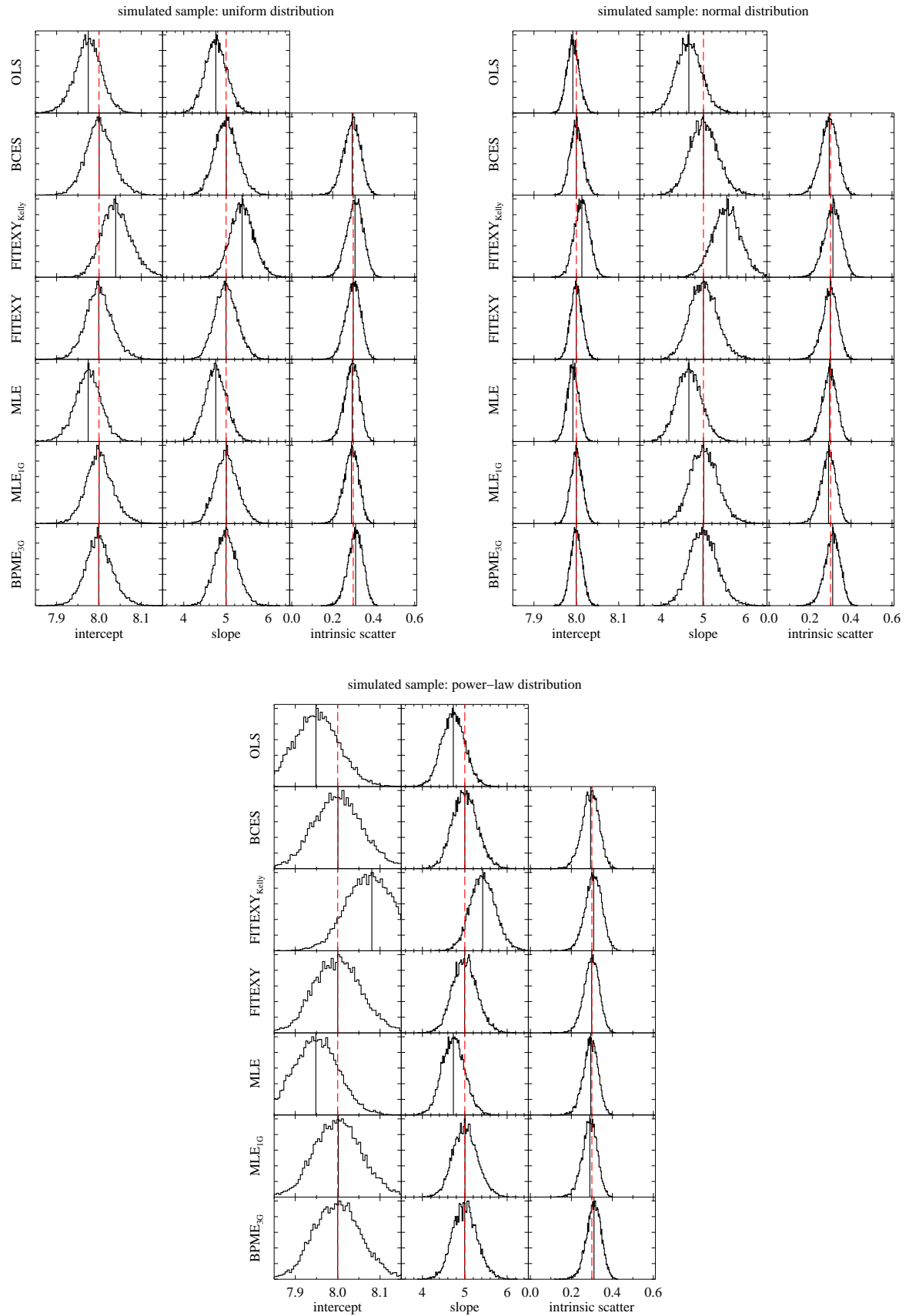


FIG. 4.— Monte Carlo simulation results for the cases of the given uniform (*upper left*), normal (*upper right*), and power-law (*bottom*) distributions on  $x$ . Each column shows the distribution of intercept, slope, and intrinsic scatter estimated from the simulated datasets using the various estimators. FITEXY<sub>Kelly</sub> is the version of FITEXY estimator implemented by Kelly (2007). MLE<sub>1G</sub> means the maximum likelihood estimator with a single Gaussian model for the distribution of independent variable as described in Section 2.4. BPME<sub>3G</sub> is the Bayesian posterior median estimate using `linmix_err` procedure based on the normal mixture model with 3 Gaussians. The median value of the simulated distribution is plotted as a vertical solid black line while the true value is indicated by the red dashed line in each panel.



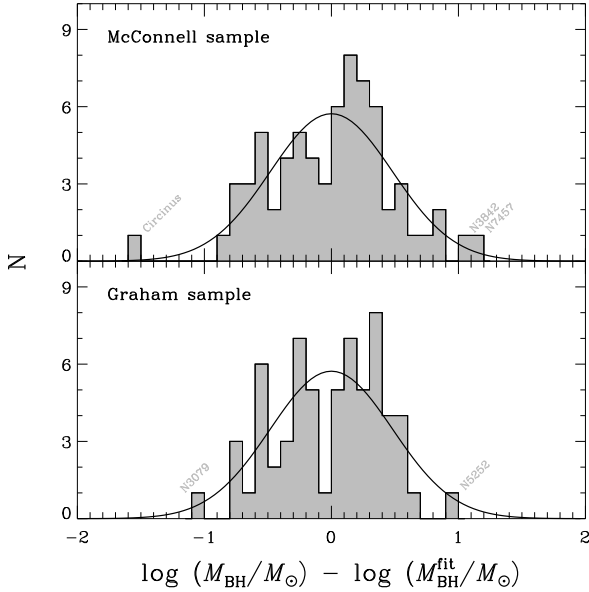


FIG. 5.— Histograms of mass residuals from the  $M_{\text{BH}} - \sigma_*$  relation based on the FITEXY estimator. A single Gaussian fit with the center fixed to zero is expressed as a solid line.

form, normal, and power-law distributions for  $x$ . The number of data points in each realization is set to be the same as that of the Graham  $M_{\text{BH}} - \sigma_*$  data set (i.e., 64). The true intercept, slope, and standard deviation of Gaussian intrinsic scatter are assumed to be 8, 5, and 0.3 dex respectively, similar to typical values from the regression results given in Table 1. In other words, the sample points ( $y$ ) from the given intrinsic relation ( $y = 8 + 5x$ ) are scattered by the Gaussian random offsets with  $\sigma = 0.3$ . Then Gaussian random noises, having zero mean and standard deviations equal to the measurement errors from the Graham et al. (2011) data set, are added to both  $x$  and  $y$ . We fit the simulated data sets using the regression methods described in Section 2.

Figure 4 shows the simulation results for the uniform, normal, and power-law distributions of  $x$ , respectively. As already pointed above, the estimated intercept and slope from MLE are biased and distributed similarly to that of the OLS estimator. This bias is regardless of the form for the intrinsic distribution, and surprisingly the MLE still has a bias for the simulated sample from the uniform distribution. This is because the the maximum-likelihood method assumes a uniform distribution for the independent variable in the range of  $-\infty$  to  $\infty$ , while in the simulations performed here the uniformly distributed data have some finite range (i.e., fixed to be same as the range of Graham et al. data). As can be seen, the true values are well recovered if the likelihood function is changed to assuming a Gaussian for the distribution of independent variables, as described in Section 2.4 (MLE<sub>1G</sub>). This modified maximum likelihood estimates give very similar distributions to that of the fully Bayesian estimates based on the `linmix_err` procedure (BPME<sub>3G</sub>). Here we also show the result of the version of FITEXY estimator used by Kelly (2007) to compare directly (FITEXY<sub>Kelly</sub>). The biased behaviour is same as noted in Kelly (2007). Thus this means that his implementation of FITEXY is inefficient compared to the one implemented here. From a viewpoint of how well the true values are recovered, all of BCES, FITEXY, and Bayesian estimators performed very well in this test.

### 3.4. The sample difference

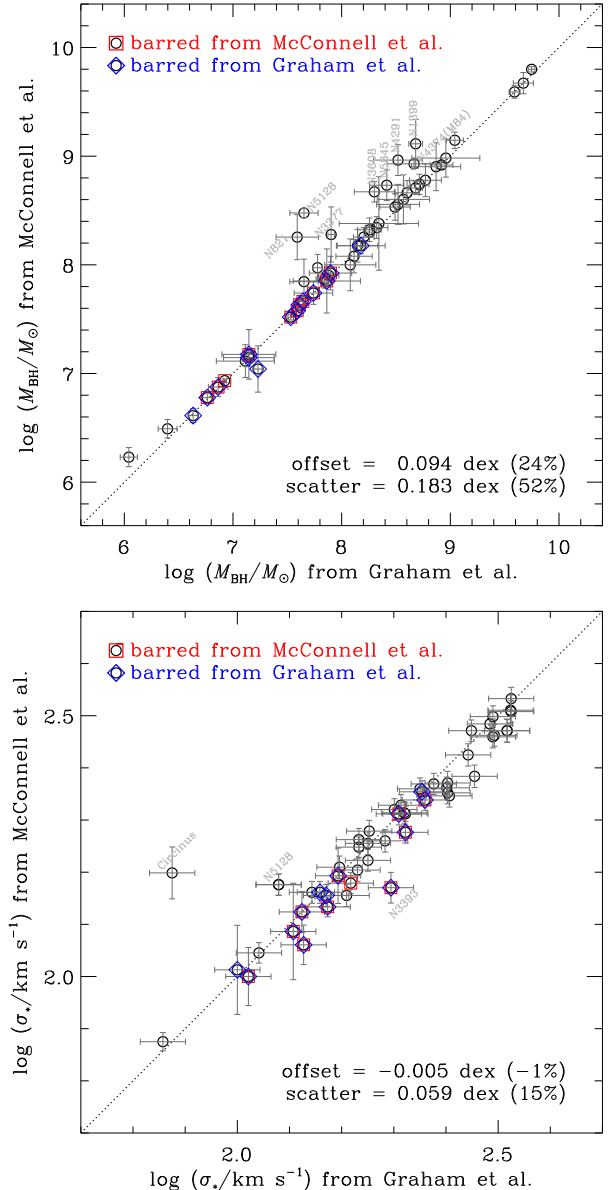


FIG. 6.— Comparison of the values of  $M_{\text{BH}}$  and  $\sigma_*$  for the galaxies in the set defined by the intersection of the McConnell et al. (2011) and Graham et al. (2011) samples. The barred sample defined by McConnell et al. (2011) is marked with a red open square, while that defined by Graham et al. (2011) is marked with a blue open diamond. The dotted line indicates the identity relationship.

In this section we investigate the sample discrepancy in detail using the most updated samples of McConnell et al. and Graham et al. We do this because the  $M_{\text{BH}} - \sigma_*$  relations derived from these two datasets show a difference in the intercept (see Table 1), which consequently affects the value of the virial factor. Note that the change in the  $M_{\text{BH}} - \sigma_*$  relation from the Gültekin sample to the McConnell sample is obvious because there was a major update of the sample as discussed in Section 3.1. However, the difference between the McConnell and Graham data is not clear since these two sample have 50 galaxies in common.

Figure 5 shows the mass residuals from the best-fit  $M_{\text{BH}} - \sigma_*$  relation derived from the McConnell and Graham data. As can be seen, there is one extreme outlier, Circinus, in the McConnell sample. Note that the central velocity dispersions of Circinus used in McConnell (i.e., 158 km/s) and Graham (i.e.,



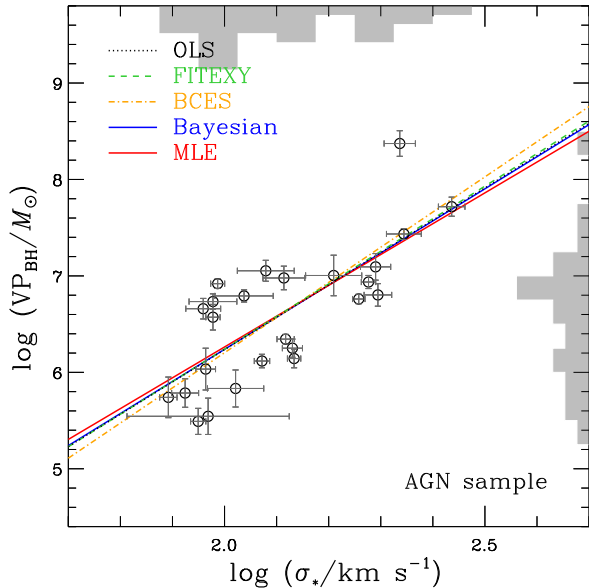


FIG. 7.— The  $VP_{\text{BH}} - \sigma_*$  relation for the AGN sample (25). As shown in the right-hand side grey histogram, we are currently suffering from a lack of high mass AGN sample. Here we can clearly see the variability of the BCES estimator due to the effect of a single point (i.e., NGC 4253) that is subject to much larger measurement error than others.

75 km/s) data are different from each other even though they were both taken from the HyperLEDA<sup>5</sup> database. The central velocity dispersion for this object currently given in the HyperLEDA is  $157.6 \pm 18.8$  km/s. We verified that the value listed by Graham et al. was a typo (Alister W. Graham 2012, private communication).

In order to investigate the difference in the sample in common between Graham and McConnell, in Figure 6 we compare the values of the black hole masses and stellar velocity dispersions. For the  $M_{\text{BH}}$  values, there are quite a few galaxies deviating from the identity relation. This is mostly due to recent updates of the black hole masses by Schulze & Gebhardt (2011) in the McConnell data. For the  $\sigma_*$ , the values of the Graham sample are slightly larger on average than those of the McConnell sample, except for a few outliers. This slight average difference stems from the difference in the adopted velocity dispersion measures. Graham et al. (2011) used the central velocity dispersion provided in HyperLEDA, while McConnell et al. (2011) mostly used the effective velocity dispersion whenever it was available. This leads to systematic differences in the dispersion values as discussed in Tremaine et al. (2002). These mass and dispersion differences work to make the intercept smaller in the Graham sample compared to the McConnell sample. However, we note that the barred sample does not show any significant difference between these datasets. We also performed the regression for the common sample only, and found that the intercepts remained almost the same while the slopes were reduced by 0.2–0.3 compared to that of the entire sample. Therefore, the difference of the intercepts between McConnell and Graham samples is due to the different values adopted for the common sample, while the difference in slopes is primarily due to the non-overlapping sample.

#### 4. THE VIRIAL FACTOR

The virial factor is of fundamental importance for estimating AGN black hole masses in that it properly calibrates the

<sup>5</sup> <http://leda.univ-lyon1.fr/>

TABLE 2  
AGN BLACK HOLE MASSES AND STELLAR VELOCITY DISPERSIONS

Galaxy	$VP_{\text{BH}}$ ( $c\tau_{\text{cent}}\sigma_{\text{line}}^2/G$ ) $10^6 M_{\odot}$	$VP_{\text{BH}}$ ref.	$\sigma_*$ $\text{km s}^{-1}$	$\sigma_*$ ref.
(1)	(2)	(3)	(4)	(5)
3C 120	$10.1^{+5.7}_{-4.1}$	1	$162 \pm 20$	2
3C 390.3	$52.2^{+11.7}_{-11.7}$	1	$273 \pm 16$	1
Ark 120	$27.2^{+3.5}_{-3.5}$	1	$221 \pm 17$	1
Arp 151	$1.31^{+0.18}_{-0.18}$	4 & 6	$118 \pm 4$	6
Mrk 50	$6.2^{+0.93}_{-0.9}$	7	$109 \pm 14$	7
Mrk 79	$9.52^{+2.61}_{-2.61}$	1	$130 \pm 12$	1
Mrk 110	$4.57^{+1.1}_{-1.1}$	1	$91 \pm 7$	3
Mrk 202	$0.55^{+0.32}_{-0.22}$	4 & 6	$78 \pm 3$	6
Mrk 279	$6.35^{+1.67}_{-1.67}$	1	$197 \pm 12$	1
Mrk 590	$8.64^{+1.94}_{-1.34}$	1	$189 \pm 6$	1
Mrk 817	$11.3^{+2.7}_{-2.8}$	5	$120 \pm 15$	1
Mrk 1310	$0.61^{+0.23}_{-0.20}$	4 & 6	$84 \pm 5$	6
NGC 3227	$1.39^{+0.29}_{-0.31}$	5	$136 \pm 4$	1
NGC 3516	$5.76^{+0.51}_{-0.59}$	5	$181 \pm 5$	1
NGC 3783	$5.42^{+0.69}_{-0.99}$	1	$95 \pm 10$	4
NGC 4051	$0.31^{+0.10}_{-0.09}$	5	$89 \pm 3$	1
NGC 4151	$8.31^{+1.04}_{-0.85}$	2	$97 \pm 3$	1
NGC 4253 (Mrk 766)	$0.35^{+0.15}_{-0.14}$	4 & 6	$93 \pm 32$	6
NGC 4593	$1.78^{+0.38}_{-0.38}$	3	$135 \pm 6$	1
NGC 4748	$0.68^{+0.24}_{-0.30}$	4 & 6	$105 \pm 13$	6
NGC 5548	$12.41^{+3.06}_{-4.21}$	4 & 6	$195 \pm 13$	6
NGC 6814	$3.73^{+1.10}_{-1.11}$	4 & 6	$95 \pm 3$	6
NGC 7469	$2.21^{+0.25}_{-0.25}$	1	$131 \pm 5$	1
PG 1426+015	$236^{+70}_{-70}$	1	$217 \pm 15$	5
SBS 1116+583A	$1.08^{+0.52}_{-0.49}$	4 & 6	$92 \pm 4$	6

NOTE. — Col. (1) name. Col. (2) virial product ( $VP_{\text{BH}} = M_{\text{BH}}/f$ ) based on the line dispersion ( $\sigma_{\text{line}}$ ) from reverberation mapping. Col. (3) reference for virial product. 1. Peterson et al. 2004; 2. Bentz et al. 2006b; 3. Denney et al. 2006; 4. Bentz et al. 2009b; 5. Denney et al. 2010; 6. Park et al. 2012; 7. Barth et al. 2011. Col. (4) stellar velocity dispersion. Col. (5) reference for stellar velocity dispersion. 1. Nelson et al. 2004; 2. Nelson & Whittle 1995; 3. Ferrarese et al. 2001; 4. Onken et al. 2004; 5. Watson et al. 2008; 6. Woo et al. 2010; 7. Barth et al. 2011.

measured virial product to a black hole mass for both the reverberation mapping method and the single-epoch method. Following Onken et al. (2004), we determine the average virial factor  $\langle f \rangle$  by forcing the AGN black hole masses onto the  $M_{\text{BH}} - \sigma_*$  relation of quiescent galaxies. The AGN sample used here is listed in Table 2 with the corresponding references. We updated the AGN sample given in Table 2 of Woo et al. (2010) by updating the virial products from Denney et al. (2010), revising the rms line widths from Park et al. (2012), and including the new  $M_{\text{BH}}$  estimate for Mrk 50 from Barth et al. (2011). In Figure 7, we estimate the  $VP_{\text{BH}} - \sigma_*$  relation with four regression methods, as in Figure 1. The regression results are listed in Table 3. The slope appears to be marginally lower than that for quiescent galaxies. This small difference in slopes might be due to noise and AGN selection effects or it could be intrinsic, indicating a difference between passive and active galaxies (see Greene & Ho 2006 and Schulze & Wisotzki 2011). Note that the current sample is not representative of the AGN population since there is a deficit of high-mass AGNs, for which stellar velocity dispersion is extremely difficult to measure due to the overwhelming AGN luminosity.

To determine the average virial factor we use the FITEXY estimator, fixing the intercept and slope to be the same as that

TABLE 3  
THE  $VP_{\text{BH}} - \sigma_*$  RELATION FOR THE ACTIVE GALAXY  
SAMPLE:  $\log(VP_{\text{BH}}/M_{\odot}) = \alpha + \beta \log(\sigma_*/200 \text{ km s}^{-1})$

Method	$\alpha$	$\beta$	$\sigma_{\text{int}}$
Forward regression			
OLS	$7.25 \pm 0.14$	$3.35 \pm 0.57$	...
MLE	$7.23 \pm 0.14$	$3.20 \pm 0.59$	$0.41 \pm 0.06$
BCES	$7.30 \pm 0.17$	$3.65 \pm 0.75$	$0.41 \pm 0.06$
FITEXY	$7.26 \pm 0.15$	$3.38 \pm 0.63$	$0.43 \pm 0.06$
Bayesian	$7.24 \pm 0.17$	$3.33 \pm 0.69$	$0.47 \pm 0.09$
Inverse regression			
OLS	$7.74 \pm 0.23$	$5.93 \pm 0.82$	...
MLE	$7.72 \pm 0.33$	$5.88 \pm 1.21$	$0.57 \pm 0.13$
BCES	$7.70 \pm 0.30$	$5.72 \pm 1.10$	$0.51 \pm 0.12$
FITEXY	$7.68 \pm 0.26$	$5.68 \pm 0.95$	$0.56 \pm 0.11$
Bayesian	$7.68 \pm 0.37$	$5.67 \pm 1.87$	$0.62 \pm 0.28$

of the  $M_{\text{BH}} - \sigma_*$  relation for the quiescent galaxies,

$$\chi^2 = \sum_{i=1}^N \frac{(y_i + \log f - \alpha - \beta x_i)^2}{\sigma_{y,i}^2 + \beta^2 \sigma_{x,i}^2 + \sigma_{\text{int}}^2}. \quad (13)$$

Here,  $y = \log(VP_{\text{BH}}/M_{\odot})$  and  $x = \log(\sigma_*/200 \text{ km s}^{-1})$ . The free parameters are only  $f$  and  $\sigma_{\text{int}}$ . Adopting the regression results listed in Table 1, we estimate the virial factor and list the result in Table 4.

Figure 8 shows the dependency of the virial factor on the adopted slope and intercept based on three datasets with four regression methods. As expected, the difference of  $f$  between the different regression methods for a particular dataset is small, with the only exception being the value of  $f$  obtained from MLE (red symbols). Estimated virial factors vary as much as a factor of 2 among the data sets, larger than the typical uncertainties. The difference in  $f$  factors derived from the McConnell and Graham data is mostly due to the difference in the values from the sample of galaxies that overlap in these two data sets, as discussed in Section 3.4. The recent updates of  $M_{\text{BH}}$  measurements by Schulze & Gebhardt (2011) lead to a smaller mean mass in the Graham sample compared to that in the McConnell sample. The difference of the adopted velocity dispersion measures results in a slightly larger velocity dispersion on average in the Graham sample compared to that of the McConnell sample. These combined differences make the intercept of the  $M_{\text{BH}} - \sigma_*$  relationship smaller in the Graham sample than in the McConnell sample, thus reducing the  $f$  factor in the Graham sample regardless of the adopted regression methods. As can be seen, the derived virial factor is susceptible to the small variation of the quiescent galaxy  $M_{\text{BH}} - \sigma_*$  relation within the current calibration process.

With the current AGN dataset, we are unable to constrain the  $f$  factor as a function of the mass range or host galaxy morphological type, since the number of sources in our sample is small and the morphology of our sample is biased toward late-type galaxies. We note that a larger AGN sample (e.g., high-mass AGNs, especially) is needed for better statistical calibration.

## 5. INVERSE FIT

In addition to the conventional forward fit relation (i.e., fitting  $M_{\text{BH}}$  for a given  $\sigma_*$ , as we performed in previous sections), Graham et al. (2011) used an inverse fit for the  $M_{\text{BH}} - \sigma_*$  relation, suggesting that it corrects for possible sample selection bias due to non-detection of intermediate-mass black holes ( $< 10^6 M_{\odot}$ ). We also follow their argument, re-

TABLE 4  
THE DERIVED AVERAGE VIRIAL FACTOR AND INTRINSIC SCATTER  
BASED ON THE ADOPTED  $M_{\text{BH}} - \sigma_*$  RELATION GIVEN IN TABLE 1

Method	$\log \langle f \rangle$	$\sigma_{\text{int}}$	$\log \langle f \rangle$	$\sigma_{\text{int}}$
From Gültekin et al. (2009) Sample				
using forward relation		using inverse relation		
MLE	$0.82 \pm 0.09$	$0.43 \pm 0.05$	$0.55 \pm 0.12$	$0.54 \pm 0.06$
BCES	$0.81 \pm 0.10$	$0.43 \pm 0.05$	$0.60 \pm 0.11$	$0.51 \pm 0.05$
FITEXY	$0.81 \pm 0.10$	$0.43 \pm 0.05$	$0.59 \pm 0.11$	$0.52 \pm 0.06$
Bayesian	$0.81 \pm 0.10$	$0.43 \pm 0.05$	$0.57 \pm 0.12$	$0.52 \pm 0.06$
From McConnell et al. (2011) Sample				
using forward relation		using inverse relation		
MLE	$0.74 \pm 0.11$	$0.48 \pm 0.05$	$0.51 \pm 0.14$	$0.62 \pm 0.07$
BCES	$0.72 \pm 0.11$	$0.49 \pm 0.05$	$0.52 \pm 0.13$	$0.62 \pm 0.07$
FITEXY	$0.71 \pm 0.11$	$0.49 \pm 0.05$	$0.53 \pm 0.13$	$0.61 \pm 0.06$
Bayesian	$0.71 \pm 0.11$	$0.49 \pm 0.05$	$0.52 \pm 0.13$	$0.61 \pm 0.07$
From Graham et al. (2011) Sample				
using forward relation		using inverse relation		
MLE	$0.64 \pm 0.10$	$0.47 \pm 0.05$	$0.42 \pm 0.13$	$0.58 \pm 0.06$
BCES	$0.55 \pm 0.11$	$0.50 \pm 0.05$	$0.42 \pm 0.13$	$0.57 \pm 0.06$
FITEXY	$0.58 \pm 0.11$	$0.49 \pm 0.05$	$0.45 \pm 0.12$	$0.56 \pm 0.06$
Bayesian	$0.58 \pm 0.11$	$0.49 \pm 0.05$	$0.46 \pm 0.12$	$0.56 \pm 0.06$

fit all relations, and derive the average virial factors based on the inverse relations (see Table 1, 3, and 4). Note that basically forward and inverse fittings are not the same in the presence of intrinsic scatter. Depending on the direction of regression (i.e., whether to choose  $M_{\text{BH}}$  or  $\sigma_*$  as the independent variable) the regressed slopes show large differences, leading to substantial changes in the virial factors. Therefore, we investigate and discuss the inverse fit in the context of the  $M_{\text{BH}} - \sigma_*$  relation. Now we have three factors related to the linear regression, which make the problem more complicated: measurement errors, intrinsic scatter, and truncation.

If there is a truncation in the y-axis (i.e.,  $\log M_{\text{BH}}$ ) as argued by Graham et al. (2011), the conventional forward fit (fit  $y$  on  $x$ ) causes a flattening in the estimated slope due to the increased loss of low mass black holes in the low  $\sigma_*$  regime (e.g., see Appendix A in Mantz et al. 2010). The inverse fit (i.e., fit  $x$  on  $y$ ) is not sensitive to this Malmquist-type bias, so long as incompleteness only exist in black hole mass. As shown by Kelly (2007), in order to avoid this selection bias on the regression result, it is necessary to assign the ‘independent variable’ as the variable used to select a sample. This approach has been generally adopted in the Tully-Fisher relation studies since its sample is magnitude-selected and errors are smaller in magnitude than in velocity (e.g., Willick 1994; Tully & Pierce 2000; Bamford et al. 2006; Weiner et al. 2006; Koen & Lombard 2009; Williams et al. 2010; Miller et al. 2011).

In our sample, the measurement errors in the truncated coordinate ( $M_{\text{BH}}$ ) are larger than in the other coordinate ( $\sigma_*$ ). Moreover, the sample selection might be highly inhomogeneous and simple selection criteria may not be sufficient for describing it. The situation is more complex in the AGN sample selection. According to Schulze & Wisotzki (2011), even though the inverse relation is insensitive to the mass-dependent selection, it does not yield the intrinsic true relation without incorporating the knowledge of the underlying host galaxy distribution function, which is currently hard to measure precisely. Furthermore, the AGN sample likely exhibits incompleteness in  $\sigma_*$  as well, as it is harder to measure  $\sigma_*$  for AGN hosting more massive black holes due to their tendency to have higher luminosities. Thus there are good

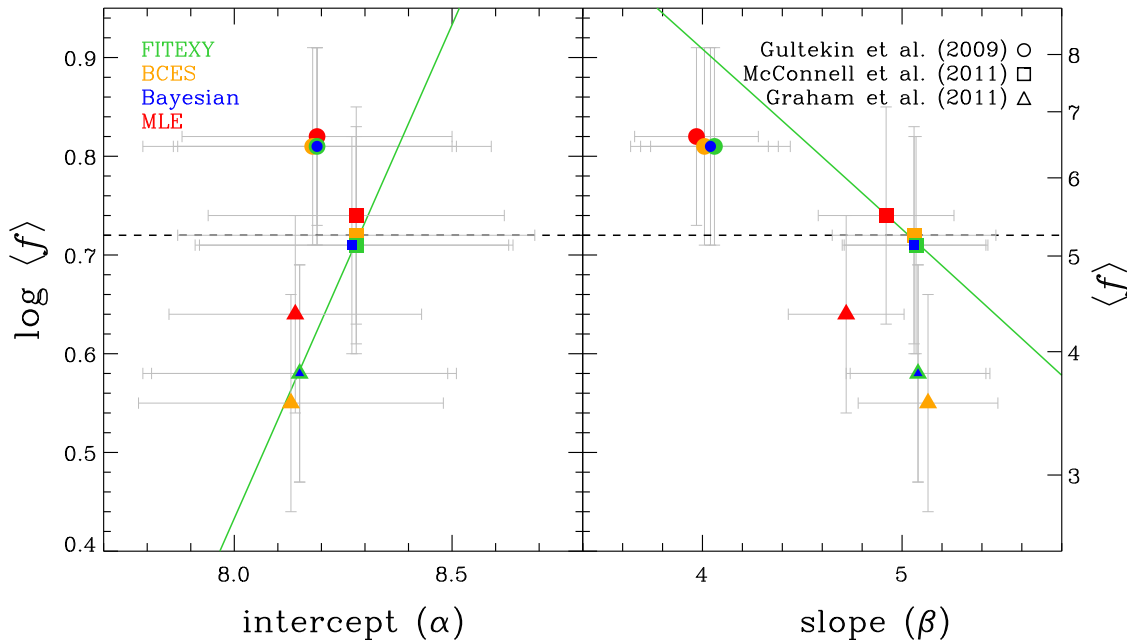


FIG. 8.— Variation of the estimated virial factor as a function of the adopted intercept (left) and slope (right) of the quiescent galaxy  $M_{\text{BH}} - \sigma_*$  relations taken from Table 1. Symbols mean the corresponding dataset used for estimation of the intercept and slope as expressed in upper right corner, while the colors of symbols indicate the regression methods used for them as given in the upper left corner. The horizontal dashed line indicates the value of the virial factor estimated from Woo et al. (2010) (i.e., 0.72). As an illustration, we add the green solid lines which show the dependence of the virial factor on the arbitrarily varied intercept (left) and slope (right) by fixing respectively the slope (left) and intercept (right) taken from the FITEXY estimates in the sample of McConnell et al. (2011).

reasons to use either type of regression, but neither of them is completely free of bias.

We provide both regression results in Table 1, 3, and 4. Inverse regression results in a steeper slope compared to that of forward regression in the  $M_{\text{BH}} - \sigma_*$  relation of quiescent galaxies. The calibration based on the inverse regression makes black hole masses inferred from the AGN virial products smaller, since most of the AGN sample is located at the low-mass regime, thus leading to a reduction in the average virial factor. This biased dependency toward the low-mass regime motivates expansion in the dynamic range of sample of AGN containing both reverberation mapping data and measurement of  $\sigma_*$ . Based on these results, we conclude that the origin of the difference in the recently reported virial factors (Woo et al. 2010 based on forward regression vs. Graham et al. 2011 based on inverse regression) is mostly due to the direction of regression adopted (i.e., whether  $M_{\text{BH}}$  is considered the independent or dependent variable), as well as the difference in the samples used to calibrate the mass estimates.

Feigelson & Babu (1992) suggested that we should choose the regression method for individual cases depending on the scientific question being investigated. Here the purpose of deriving the  $M_{\text{BH}} - \sigma_*$  relation for local quiescent galaxies is to calibrate AGN black hole masses with determining the virial factor. By properly comparing the black hole masses of inactive galaxies to virial products of active galaxies, the average virial factor is constrained as discussed in the previous section. Thus it is desirable to adopt the type of regression which yields the relation that minimizes the scatter in the black hole mass estimates (Graham & Driver 2007). It is more common to adopt the host spheroidal quantity as the independent variable because the scaling relations are often used to infer black hole mass using the host spheroidal quantities as a proxy. Considering this, and the fact that the AGN sample likely suffers from Malmquist bias in both  $M_{\text{BH}}$  and  $\sigma_*$ , we prefer the calibration from the traditional forward regression.

## 6. DISCUSSION AND CONCLUSIONS

We investigated the differences in the derived  $M_{\text{BH}} - \sigma_*$  relation and virial factor using the recently compiled datasets of quiescent and active galaxies. The investigated possible origins of the difference are the fitting methodology and the sample difference.

For the difference in regression methods, we utilized and compared four linear regression techniques: FITEXY, Bayesian, BCES, and Maximum likelihood. With the current level of measurement errors of the  $M_{\text{BH}} - \sigma_*$  dataset, all estimators except for the maximum likelihood estimator show good performance and consistent results with each other. There is no significant difference between the estimators. However, the assigned size of measurement errors on  $\sigma_*$  can have a significant impact on the regression results, especially for the BCES and Maximum likelihood estimators. The Maximum likelihood method using an implicit assumption of a uniform distribution for the intrinsic distribution of the independent variables introduces a bias which is clearly noticeable when the measurement errors on the independent variable are large (e.g., above 10% errors in the Graham sample as shown in Figure 2). Without properly accounting for the form of the intrinsic distribution of the independent variable, MLE estimates are very similar to the OLS results. Therefore we do not recommend this method for regression analysis in general. Of course for the  $M_{\text{BH}} - \sigma_*$  regression analysis the difference in the estimated slope is only marginal at the current adopted level of uncertainty on  $\sigma_*$  (5%). The BCES estimator is also one of the good estimators based on the current measurement error level on  $\sigma_*$ , although it may be problematic if the error is larger. Based on our simulation results, the FITEXY estimator shows slightly better performance and the least-biased result compared to the other methods, although the others also perform well and the differences are marginal. This is consistent with the result of Novak et al. (2006), although they did not provide an explicit imple-

mentation of all of the methods, nor a specific quantitative comparison. In general, we recommend both the FITEXY and Bayesian estimators, although the latter is computationally more intensive, especially when the measurement errors are large. However, we note that the Bayesian estimator has the advantage over the method of FITEXY in that it calculates the full probability distribution function (i.e., posterior) of the parameters for the given data, and hence provides well-defined and reliable parameter uncertainties. In addition, the Bayesian method can incorporate upper limits, as can the method of Gültekin et al. (2009), whereas the FITEXY cannot. If we perform the regression using the Bayesian method, for the Gültekin sample including upper limits as well as secure measurements, the result changes from ( $\alpha = 8.19 \pm 0.07$ ,  $\beta = 4.04 \pm 0.40$ ,  $\sigma_{\text{int}} = 0.42 \pm 0.05$ ) to ( $\alpha = 8.13 \pm 0.07$ ,  $\beta = 4.32 \pm 0.38$ ,  $\sigma_{\text{int}} = 0.43 \pm 0.05$ ), thus  $\log \langle f \rangle$  correspondingly decreases from  $0.81 \pm 0.10$  to  $0.70 \pm 0.10$ . As discussed in Tremaine et al. (2002), accurate and consistent estimation of an individual stellar velocity dispersion with a correct measurement uncertainty is still required and it will be an important factor for better constraining the  $M_{\text{BH}} - \sigma_*$  relation and virial factor.

The difference in sample is the most important factor contributing to the differences in derived  $M_{\text{BH}} - \sigma_*$  relations. Gültekin et al. (2009) noted that the late-type galaxy and pseudobulge population in their sample is the source of the difference in intrinsic scatter measurements by comparing their sample to that of Tremaine et al. (2002). Greene et al. (2010) found that the late-type low-mass galaxies show large scatter and are offset relative to the  $M_{\text{BH}} - \sigma_*$  relation of elliptical galaxies using the sample of megamaser disk galaxies. By extending the work of Graham et al. (2008), recently Graham et al. (2011) showed that the fraction of barred galaxies in their sample alters the  $M_{\text{BH}} - \sigma_*$  relationship by dividing their sample into barred and non-barred galaxies.

According to these previous studies, the  $M_{\text{BH}} - \sigma_*$  relation seems to be not universal. It varies depending on the mass range and galaxy type. Correspondingly, the average  $f$  factor is also significantly affected by the sample population, since the intercept and slope from the quiescent galaxy  $M_{\text{BH}} - \sigma_*$  relation are directly used in the calibration process. As investigated in this study, the differences in the adopted sample contribute to the change of the virial factor. Moreover, the direction of regression (forward vs. inverse) causes further changes in the virial factor. We showed that the derived  $f$  factors vary as much as a factor of 2, which is from a combined effect of the sample and regression used. These differences could be thought of as an additional systematic uncertainty in the AGN black hole mass estimation via the current calibration process of the virial factor, since there is no obvious physical foundation for the selection of the appropriate sample and direction of regression.

The true average  $f$  factor should not be changed by the host galaxy type since there should be no direct physical link between the AGN BLR geometry and the global morphology of host galaxies. Unfortunately, the estimated average  $f$  factor may be subject to biases due to its calibration based on a single  $M_{\text{BH}} - \sigma_*$  relationship. However, since the current sample is not large enough to calibrate the virial factor as a function of galaxy type, it is better to use a single value of the mean  $f$  factor for AGN  $M_{\text{BH}}$  estimation in order to avoid additional systematic errors until we get enough direct measurements of the structure of the BLR for an each individual AGN. We note that an alternative method to measure AGN black hole mass that derives the virial factor through BLR modeling has been recently developed and applied to the reverberation data (e.g.,

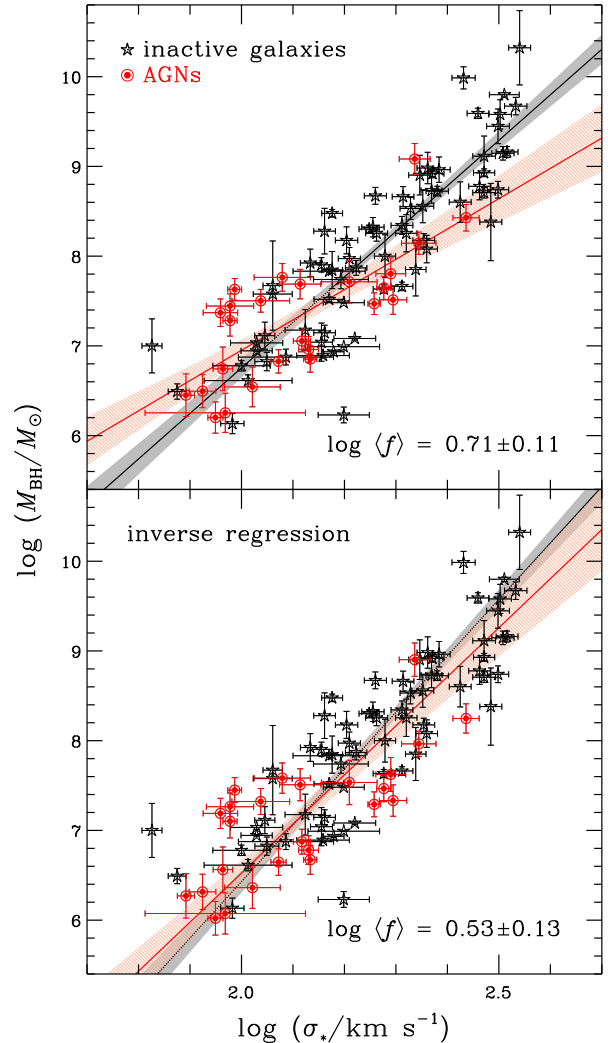


FIG. 9.— The updated  $M_{\text{BH}} - \sigma_*$  relations for the inactive (black) and active (red) samples using the FITEXY estimator for the forward regression (upper) and inverse regression (lower). Shaded regions show the  $1\sigma$  (68%) confidence intervals on the best-fit line. The inactive sample is from McConnell et al. (2011) and is the most recent one. The active sample is given in Table 2.

Pancoast, Brewer, & Treu 2011; Brewer et al. 2011; Pancoast et al. 2012). Given the uncertainties in the  $f$  factor, when investigating evolutionary trends in the  $M_{\text{BH}} - \sigma_*$  relation based on SE estimates, we recommend to use self-consistent samples and techniques at different redshifts. In other words, one should measure the SE black hole masses consistently for AGN samples at different redshifts by using the cross-calibrated recipes based on the same virial factor. In this way the virial factor should be very similar for all samples and cancel out in the determination of the evolution of  $\log M_{\text{BH}}$  under the assumption that the virial factor is not a function of redshift (e.g., Woo et al. 2008).

Finally, we present the updated  $M_{\text{BH}} - \sigma_*$  relation for local active galaxies based on the FITEXY estimator in Figure 9, where the forward (inverse) regression result is  $\alpha = 7.97 \pm 0.14$ ,  $\beta = 3.38 \pm 0.61$ , and  $\sigma_{\text{int}} = 0.42 \pm 0.06$  ( $\alpha = 8.17 \pm 0.27$ ,  $\beta = 5.47 \pm 1.01$ , and  $\sigma_{\text{int}} = 0.52 \pm 0.11$ ). The AGN black hole masses were converted from the virial products using the virial factor  $\log \langle f \rangle = 0.71 \pm 0.11$  ( $\log \langle f \rangle = 0.53 \pm 0.13$ ) derived in Section 4. From a methodological point of view, we prefer the forward regression as discussed in Section 5. Thus our preferred value for the virial factor is 0.71 based on the

preferred forward FITEXY/Bayesian estimation with the most recent sample (McConnell et al. 2011). This value is consistent with that of Woo et al. (2010) (i.e., 0.72) and differs from that of Graham et al. (2011) (i.e., 0.45) by  $\sim 0.26$  dex. The difference arises from the combination of sample differences and regression differences. It is worth noticing that the bottom panel of Figure 9 shows slightly better agreement between the non-AGN and AGN  $M_{\text{BH}} - \sigma_*$  relations, which may indicate that the inverse regression has less bias than the forward one and thus might be more reliable. However, this conclusion only holds if we assume that the active and inactive galaxies share the same  $M_{\text{BH}} - \sigma_*$  relationship. Considering these issues, it is still not conclusive whether the inverse method is preferable with the current datasets owing

to selection effects and limited dynamic range of the AGN sample.

This work was supported by the National Research Foundation of Korea (NRF) grant funded by the Korea government (MEST) (No. 2012-006087). DP would like to thank Hyung Mok Lee, Matthew W. Auger, Jong Chul Lee, and Andreas Schulze for helpful discussions. BK acknowledges support from the Southern California Center for Galaxy Evolution, a multi-campus research program funded by the University of California Office of Research. TT acknowledges support from the Packard Foundation through a Packard research fellowship. We thank the anonymous referee for constructive comments and suggestions.

## REFERENCES

- Akritas, M. G., & Bershad, M. A. 1996, *ApJ*, 470, 706  
 Auger, M. W., Treu, T., Bolton, A. S., et al. 2010, *ApJ*, 724, 511  
 Bamford, S. P., Aragón-Salamanca, A., & Milvang-Jensen, B. 2006, *MNRAS*, 366, 308  
 Barth, A. J., Pancoast, A., Thorman, S. J., et al. 2011, *ApJ*, 743, L4  
 Batcheldor, D. 2010, *ApJ*, 711, L108  
 Bedregal, A. G., Aragón-Salamanca, A., & Merrifield, M. R. 2006, *MNRAS*, 373, 1125  
 Beifiori, A., Courteau, S., Corsini, E. M., & Zhu, Y. 2012, *MNRAS*, 419, 2497  
 Bennert, V. N., Treu, T., Woo, J.-H., et al. 2010, *ApJ*, 708, 1507  
 Bentz, M. C., Peterson, B. M., Pogge, R. W., Vestergaard, M., & Onken, C. A. 2006a, *ApJ*, 644, 133  
 Bentz, M. C., Denney, K. D., Cackett, E. M., et al. 2006b, *ApJ*, 651, 775  
 Bentz, M. C., Peterson, B. M., Pogge, R. W., & Vestergaard, M. 2009a, *ApJ*, 694, L166  
 Bentz, M. C., Walsh, J. L., Barth, A. J., et al. 2009b, *ApJ*, 705, 199  
 Blandford, R. D., & McKee, C. F. 1982, *ApJ*, 255, 419  
 Booth, C. M., & Schaye, J. 2009, *MNRAS*, 398, 53  
 Bower, R. G., Benson, A. J., Malbon, R., et al. 2006, *MNRAS*, 370, 645  
 Brewer, B. J., Treu, T., Pancoast, A., et al. 2011, *ApJ*, 733, L33  
 Caimmi, R. 2011a, *NewA*, 16, 337  
 Caimmi, R. 2011b, arXiv:1111.2680  
 Cheng, C. L., & Riu, J. 2006, *Technometrics*, 48, 511  
 Croton, D. J., Springel, V., White, S. D. M., et al. 2006, *MNRAS*, 365, 11  
 Di Matteo, T., Springel, V., & Hernquist, L. 2005, *Nature*, 433, 604  
 Denney, K. D., Bentz, M. C., Peterson, B. M., et al. 2006, *ApJ*, 653, 152  
 Denney, K. D., Watson, L. C., Peterson, B. M., et al. 2009, *ApJ*, 702, 1353  
 Denney, K. D., Peterson, B. M., Pogge, R. W., et al. 2010, *ApJ*, 721, 715  
 Fabian, A. C. 1999, *MNRAS*, 308, L39  
 Feigelson, E. D., & Babu, G. J. 1992, *ApJ*, 397, 55  
 Ferrarese, L., & Ford, H. 2005, *Space Sci. Rev.*, 116, 523  
 Ferrarese, L., & Merritt, D. 2000, *ApJ*, 539, L9  
 Ferrarese, L., Pogge, R. W., Peterson, B. M., et al. 2001, *ApJ*, 555, L79  
 Gebhardt, K., Bender, R., Bower, G., et al. 2000, *ApJ*, 539, L13  
 Gebhardt, K., & Thomas, J. 2009, *ApJ*, 700, 1690  
 Graham, A. W. 2008, *ApJ*, 680, 143  
 Graham, A. W., & Driver, S. P. 2007, *ApJ*, 655, 77  
 Graham, A. W., Onken, C. A., Athanassoula, E., & Combes, F. 2011, *MNRAS*, 412, 2211  
 Greene, J. E., & Ho, L. C. 2006, *ApJ*, 641, L21  
 Greene, J. E., Peng, C. Y., Kim, M., et al. 2010, *ApJ*, 721, 26  
 Gull, S. F. 1989, *Bayesian Data Analysis: Straight-line fitting*, in *Maximum Entropy and Bayesian Methods*, ed. J. Skilling, (Dordrecht:Kluwer Academic Publishers) 511  
 Gültekin, K., Richstone, D. O., Gebhardt, K., et al. 2009, *ApJ*, 698, 198  
 Gültekin, K., Tremaine, S., Loeb, A., & Richstone, D. O. 2011, *ApJ*, 738, 17  
 Häring, N., & Rix, H.-W. 2004, *ApJ*, 604, L89  
 Hogg, D. W., Bovy, J., & Lang, D. 2010, arXiv:1008.4686  
 Hopkins, P. F., Hernquist, L., Cox, T. J., et al. 2006, *ApJS*, 163, 1  
 Hu, J. 2008, *MNRAS*, 386, 2242  
 Isobe, T., Feigelson, E. D., Akritas, M. G., & Babu, G. J. 1990, *ApJ*, 364, 104  
 Jiang, Y.-F., Greene, J. E., & Ho, L. C. 2011, *ApJ*, 737, L45  
 Kaspi, S., Smith, P. S., Netzer, H., et al. 2000, *ApJ*, 533, 631  
 Kaspi, S., Maoz, D., Netzer, H., et al. 2005, *ApJ*, 629, 61  
 Kauffmann, G., & Haehnelt, M. 2000, *MNRAS*, 311, 576  
 Kelly, B. C. 2007, *ApJ*, 665, 1489  
 Kelly, B. C. 2011, arXiv:1112.1745  
 Kim, M., Ho, L. C., Peng, C. Y., et al. 2008, *ApJ*, 687, 767  
 Koen, C., & Lombard, F. 2009, *MNRAS*, 395, 1657  
 Körding, E., Falcke, H., & Corbel, S. 2006, *A&A*, 456, 439  
 Kormendy, J., Bender, R., & Cornell, M. E. 2011, *Nature*, 469, 374  
 Kormendy, J., & Richstone, D. 1995, *ARA&A*, 33, 581  
 Li, G., Conroy, C., & Loeb, A. 2011, arXiv:1110.0017  
 Magorrian, J., Tremaine, S., Richstone, D., et al. 1998, *AJ*, 115, 2285  
 Mancini, L., & Feoli, A. 2012, *A&A*, 537, A48  
 Mantz, A., Allen, S. W., Ebeling, H., Rapetti, D., & Drlica-Wagner, A. 2010, *MNRAS*, 406, 1773  
 March, M. C., Trotta, R., Berkes, P., Starkman, G. D., & Vaudrevange, P. M. 2011, *MNRAS*, 418, 2308  
 Marconi, A., Axon, D. J., Maiolino, R., et al. 2008, *ApJ*, 678, 693  
 Marconi, A., & Hunt, L. K. 2003, *ApJ*, 589, L21  
 Markwardt, C. B. 2009, *Astronomical Data Analysis Software and Systems XVIII*, 411, 251  
 McConnell, N. J., Ma, C.-P., Gebhardt, K., et al. 2011, *Nature*, 480, 215  
 McLure, R. J., & Dunlop, J. S. 2002, *MNRAS*, 331, 795  
 Merritt, D., & Ferrarese, L. 2001, *ApJ*, 547, 140  
 Miller, S. H., Bundy, K., Sullivan, M., Ellis, R. S., & Treu, T. 2011, *ApJ*, 741, 115  
 Nelson, C. H., Green, R. F., Bower, G., Gebhardt, K., & Weistrop, D. 2004, *ApJ*, 615, 652  
 Nelson, C. H., & Whittle, M. 1995, *ApJS*, 99, 67  
 Novak, G. S., Faber, S. M., & Dekel, A. 2006, *ApJ*, 637, 96  
 Onken, C. A., Ferrarese, L., Merritt, D., et al. 2004, *ApJ*, 615, 645  
 Pancoast, A., Brewer, B. J., & Treu, T. 2011, *ApJ*, 730, 139  
 Pancoast, A., Brewer, B. J., Treu, T., et al. 2012, *ApJ*, 754, 49  
 Park, D., Woo, J.-H., Treu, T., et al. 2012, *ApJ*, 747, 30  
 Peterson, B. M. 1993, *PASP*, 105, 247  
 Peterson, B. M., Ferrarese, L., Gilbert, K. M., et al. 2004, *ApJ*, 613, 682  
 Press, W. H., Teukolsky, S. A., Vetterling, W. T., & Flannery, B. P. 1992, *Numerical recipes in C. The art of scientific computing*, Cambridge: University Press, 2nd ed.  
 Richstone, D., Ajhar, E. A., Bender, R., et al. 1998, *Nature*, 395, A14  
 Sani, E., Marconi, A., Hunt, L. K., & Risaliti, G. 2011, *MNRAS*, 413, 1479  
 Schulze, A., & Gebhardt, K. 2011, *ApJ*, 729, 21  
 Schulze, A., & Wisotzki, L. 2011, *A&A*, 535, A87  
 Shen, J., & Gebhardt, K. 2010, *ApJ*, 711, 484  
 Silk, J., & Rees, M. J. 1998, *A&A*, 331, L1  
 Somerville, R. S., Hopkins, P. F., Cox, T. J., Robertson, B. E., & Hernquist, L. 2008, *MNRAS*, 391, 481  
 Tremaine, S., Gebhardt, K., Bender, R., et al. 2002, *ApJ*, 574, 740  
 Tully, R. B., & Pierce, M. J. 2000, *ApJ*, 533, 744  
 van den Bosch, R. C. E., & de Zeeuw, P. T. 2010, *MNRAS*, 401, 1770  
 Vika, M., Driver, S. P., Cameron, E., Kelvin, L., & Robotham, A. 2012, *MNRAS*, 419, 2264  
 Wandel, A., Peterson, B. M., & Malkan, M. A. 1999, *ApJ*, 526, 579  
 Watson, L. C., Martini, P., Dasya, K. M., et al. 2008, *ApJ*, 682, L21  
 Weiner, B. J., Willmer, C. N. A., Faber, S. M., et al. 2006, *ApJ*, 653, 1049  
 Williams, M. J., Bureau, M., & Cappellari, M. 2010, *MNRAS*, 409, 1330  
 Willick, J. A. 1994, *ApJS*, 92, 1  
 Woo, J.-H., Treu, T., Malkan, M. A., & Blandford, R. D. 2008, *ApJ*, 681, 925  
 Woo, J.-H., Treu, T., Barth, A. J., et al. 2010, *ApJ*, 716, 269  
 Xiao, T., Barth, A. J., Greene, J. E., et al. 2011, *ApJ*, 739, 28